



Direction-Dependent Thermoelectric Properties of a Layered Compound In_2Te_5 Single Crystal

Anup V. Sanchela^{1,2} · Ajay D. Thakur³ · C. V. Tomy²

Received: 26 June 2021 / Accepted: 28 January 2022 / Published online: 21 February 2022
© The Minerals, Metals & Materials Society 2022

Abstract

We examine the anisotropic electrical and thermal transport properties in single crystals of In_2Te_5 belonging to the monoclinic space group $C12/c1$ with the temperature gradient applied parallel (\parallel) and perpendicular (\perp) to the crystallographic c -axis of the crystals. A systematic investigation of structural, electrical, and thermal properties suggests the role of layered structure in this material in guiding its thermoelectric behavior. The thermal conductivity along the c -axis ($\kappa_{\parallel c}$) was found to be smaller by a factor of 2 compared to the thermal conductivity along the direction perpendicular to the c -axis ($\kappa_{\perp c}$) over the entire temperature range. In contrast, the Seebeck coefficient along the c -axis ($S_{\parallel c}$) was found to be higher than its value along the direction perpendicular to the c -axis ($S_{\perp c}$). At room temperature, the figure of merit $zT_{\parallel c}$ is found to be four times larger as compared to the figure of merit $zT_{\perp c}$. Our results provide insights into how the resistivity, thermal conductivity, and thermopower depends on the crystalline anisotropy and its impact on the overall zT .

Keywords Anisotropy · single crystal · Seebeck coefficient · thermal conductivity · layered structure

Introduction

Over the past few decades, thermoelectric materials have attracted considerable research interest because of their possible applications in direct solid-state energy conversion between waste heat and electrical power (using thermoelectric generators), as well as for the purpose of electronic refrigeration.^{1–4} The dimensionless figure of merit, $zT = S^2T/\rho(\kappa_l + \kappa_e)$, can be used to quantify thermoelectric material performance. Here, S is the thermopower, ρ is the electrical resistivity, κ_l is the lattice thermal conductivity, κ_e is the electronic thermal conductivity, and T is the absolute temperature, such that a large zT value is desirable for improving the efficiency of thermoelectric generators and coolers. Over the past few years, several strategies have been applied to reduce the lattice thermal conductivity, such as

disordering the system by introducing point defects,⁵ creating resonant scattering by localized rattling atoms,^{4,6–8} creating maximum interfaces by ball milling and hot pressing/spark plasma sintering (SPS),^{4,6,9} introducing nanoscale precipitates in thermoelectric materials, and¹⁰ synthesizing nanosheets.¹¹ Utilizing the aforementioned techniques, it is found to be possible to increase phonon scattering, thereby minimizing lattice thermal conductivity.

Anisotropy is another important parameter that plays a crucial role in enhancing the zT values in thermoelectric materials. Layered compounds are the natural choice for exploiting this effect, and hence, the direction-dependent thermoelectric properties have been investigated in detail in many-layered compounds. A few of these layered compounds, which are considered high performance layered thermoelectric materials, are CsBi_4Te_6 , Ag_2Te , Bi_2Te_3 , and SnSe . CsBi_4Te_6 crystallizes in a monoclinic structure (space group $C2/m$) and has lattice parameters of $a = 51.9 \text{ \AA}$, $b = 4.4 \text{ \AA}$ and $c = 14.5 \text{ \AA}$. The crystal structure is comprised of alternating slabs of Bi_4Te_6 , separated by layered Cs^+ ions (see Fig. 1a). This type of unique structure prevents the motion of Cs^+ atoms along the perpendicular crystallographic b -axis. The localized Cs^+ ions behave like rattlers, and the resonant scattering of phonons from these rattlers reduces the lattice thermal conductivity. Hence, the zT value

✉ Anup V. Sanchela
anup.sanchela@sot.pdpu.ac.in

¹ Department of Physics, Pandit Deendayal Energy University, Raysan, Gandhinagar 382007, India

² Department of Physics, Indian Institute of Technology Bombay, Powai, Mumbai 400076, India

³ Department of Physics, Indian Institute of Technology Patna, Bihta 801106, India

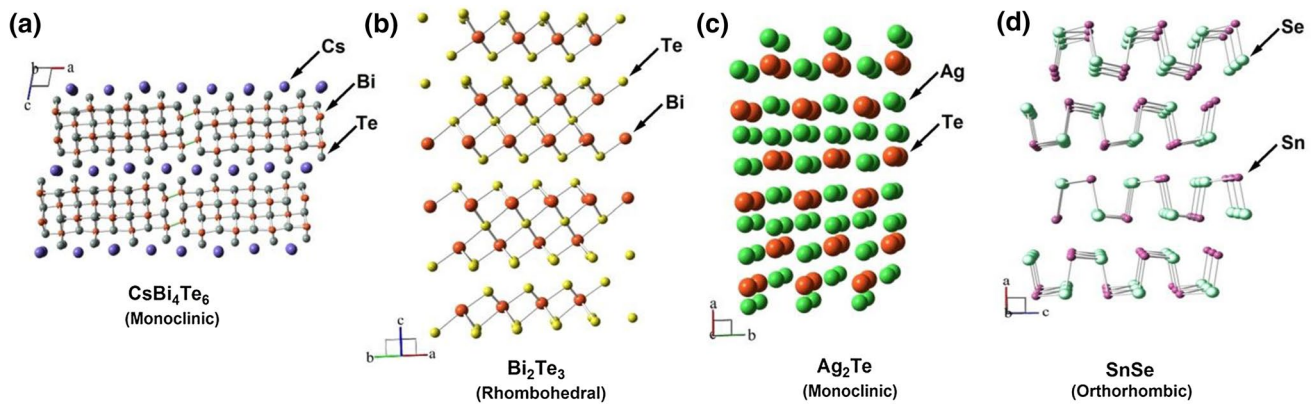


Fig. 1 The crystal structures of (a) CsBi_4Te_6 (b) Bi_2Te_3 (c) Ag_2Te , and (d) SnSe .

reaches ~ 0.8 at 225 K in doped CsBi_4Te_6 .^{6,12,13} Similarly, Bi_2Te_3 is rhombohedral with lattice parameters, $a = 4.38 \text{ \AA}$ and $b = 30.50 \text{ \AA}$.¹⁴ The crystal structure consists of atomic sheets in the a - b plane with Te1-Bi-Te2-Bi-Te1 quintets (see Fig. 1b). These sheets are held together only by a weak van der Waals force along the c -axis. Therefore, Bi_2Te_3 possesses a structural anisotropy. Poudel et al.⁹ reported a maximum zT value of 1.4 at 373K in p -type $\text{Bi}_{2-x}\text{Sb}_x\text{Te}_3$ samples. Yan et al.¹⁵ reported zT values in the range of 0.85 to 1.04 at 398K in n -type $\text{Bi}_2\text{Te}_{3-x}\text{Se}_x$ samples.^{12,16} Additionally, Ag_2Te crystallizes in the monoclinic structure with a $P21/c$ space group and the lattice parameters are $a = 8.16 \text{ \AA}$, $b = 4.46 \text{ \AA}$, and $c = 8.97 \text{ \AA}$. The structure consists of triple layers; the top and bottom layers comprise alternating pairs of Ag and Te atoms, and the middle layer consists of only Ag atoms (see Fig. 1c).¹⁷ This β - Ag_2Te (monoclinic structure) phase transforms into α - Ag_2Te (FCC cubic structure) phase at 417 K. α - Ag_2Te is also known as an Ag-ion conductor since the Ag ions start hopping to the interstitial sites when the phase transition begins. This hopping not only enhances the electrical conductivity but also reduces the lattice thermal conductivity.¹⁸ Lee et al. found a high zT value of 1.5 at 700K in bulk composites $\text{Sb}_2\text{Te}_3/\text{Ag}_2\text{Te}$.¹⁹ Another layered compound, SnSe reported by Zhao et al., exhibits an ultra-low thermal conductivity and a very high zT of ~ 2.6 along the b -axis. Because of anisotropy, the zT is ~ 2.3 along the c -axis and 0.8 along the a -axis. At room temperature, SnSe forms a layered orthorhombic structure with space group $Pnma$.²⁰ The crystal structure of SnSe possesses eight atoms (two adjacent double layers) in one primitive cell. The unique atomic stacking and anisotropic zigzag structures (see Fig. 1d) are responsible for the ultra-low thermal conductivity and high zT in SnSe .^{21,22} Thus, the aforementioned four compounds have a common feature, viz., a layered structure. Further, Cs^+ ions act as rattlers, which produce resonant scattering in CsBi_4Te_6 and minimize the thermal conductivity. Similarly, thermal conductivity

reduction occurred due to Te1-Bi-Te2-Bi-Te1 quintets in Bi_2Te_3 and Ag ion hopping in Ag_2Te , respectively. Furthermore, the zigzag structure of SnSe assists in achieving an ultra-low thermal conductivity. These results suggest that there is always a thermoelectric property improvement in materials with layered structure.

In_2Te_5 is a compound that is reported to have a natural layered structure. The In_2Te_5 structure was solved by Walton et al.,²³ and it was found that In_2Te_5 crystallizes in two different space groups, Cc and $C12/c1$. The structure with space group Cc (labeled as In_2Te_5 (I)) results in lattice parameters $a = 4.39 \text{ \AA}$, $b = 16.39 \text{ \AA}$, and $c = 13.52 \text{ \AA}$, whereas the structure with space group $C12/c1$ (In_2Te_5 (II)) forms with cell parameters $a = 16.66 \text{ \AA}$, $b = 4.36 \text{ \AA}$ and $c = 41.34 \text{ \AA}$. In order to explore how the zigzag layered structure of In_2Te_5 affects the thermoelectric properties followed by zT improvement from low temperatures to room temperature, we have prepared the In_2Te_5 (II) phase ($C12/c1$ phase), which is confirmed by the Rietveld refinement analysis.²³ We have investigated the anisotropic thermoelectric properties of this monoclinic compound (space group $C12/c1$) by preparing single crystals. We show that a suitable choice of the thermal gradient direction improves lattice thermal conductivity and thermopower near room temperature, resulting in an increase in the figure of merit zT .²⁴ These findings are useful because groups III and VI semiconducting materials are used in practical applications such as heterojunction development, optoelectronic components, and Schottky barriers.²⁵

Experimental Details

Single crystals of In_2Te_5 were grown by the modified Bridgman method. In (99.99%) and Te shots (99.99%) were weighed in a stoichiometric ratio and sealed in a quartz ampoule after evacuation (10^{-5} mbar). The charge

was heated to 500°C over a time period of 15 h, kept at this temperature for 24 h, and then cooled slowly (2°C/h) to 470°C where it was left for 24 h.^{25,26} The charge was then furnace-cooled to room temperature. Well-grown single crystals could easily be separated from the charge for various measurements. The typical dimensions of the single crystals chosen for the present study are $4.54 \times 1.96 \times 1.27 \text{ mm}^3$. Powder x-ray diffraction patterns were obtained using an x-ray diffraction (XRD) system (Philips X'Pert Pro, the Netherlands) with Cu K α radiation. The thermo-power and thermal conductivity were measured by using the Thermal Transport Option (TTO) in a Physical Property Measurement System (PPMS; Quantum Design Inc., USA). Four-probe resistivity and heat capacity measurements were performed using the Resistivity and Heat Capacity Option (PPMS; Quantum Design Inc., USA). The typical accuracy is $\pm 5\%$, as per the PPMS specifications. The nominal composition was examined by energy dispersive x-ray analysis. The observed stoichiometric values were found to be within 1.5% of the starting composition. The single-crystal morphology was checked with a field emission scanning electron microscope (FESEM), and the single-crystalline nature was confirmed by a high-resolution transmission electron microscope (HRTEM).

Results and Discussion

Material Characterization

X-ray Diffraction

Figure 2a shows the XRD pattern of the powdered single crystals of In_2Te_5 . Rietveld refinement was performed on the obtained pattern using the known monoclinic structure with space group $C12/c1$. All the observed peaks could be indexed, and a good agreement between the experimental data (open circles) and the calculated pattern (solid line) suggests the formation of In_2Te_5 in a single phase. In order to determine the orientation of the single crystals used for the present studies, x-ray diffraction patterns were obtained from the single crystals. One such pattern is shown in Fig. 2b. It is clear from the pattern that the crystal planes are grown along the c -direction (it can be noted clearly that only the $[0, 0, 6]$ and $[0, 0, 12]$ diffractions are seen in the measured 2θ range).

TEM Analysis

We show in Fig. 3a the structure of In_2Te_5 . The dark pink and dark blue spheres represent the indium and tellurium atoms, respectively. The structure consists of In-Te rings interconnected by three cross-linked Te atoms along the plane.³¹ These In-Te planes are stacked along the

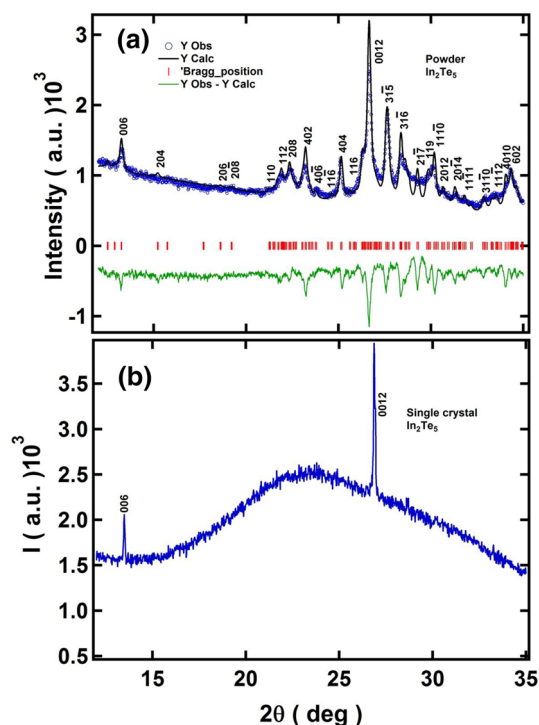


Fig. 2 (a) Powder x-ray diffraction pattern of In_2Te_5 with the details of Rietveld refinement. (b) x-ray diffraction pattern for a single crystal of In_2Te_5 .

crystallographic c -axis to form a unit cell. Such a structure has been seen to possess a large unit cell with very different lattice parameters^{12,23}. Figure 3b shows the selected area electron diffraction (SAED) pattern obtained for one of the single crystals used in our measurements. The characteristic bright spots indicating the single-crystalline nature of the specimen are evident. From the HRTEM photograph (Fig. 3c), the lattice spacing between the two neighbouring atomic planes was estimated to be about 3.38Å (marked by two parallel lines), which is very close to the reported interplanar distance of 3.39Å between the two adjacent $(0,0,12)$ planes (JCPDS #00-031-0602). Figure 3d shows the optical micrograph of a cleaved piece of a single crystal belonging to the same batch where the layered structure of the single crystal In_2Te_5 is clearly visible. A summary of the crystallographic data is given in Table I.

Electrical Resistivity

The temperature dependence of the electrical resistivity $\rho(T)$ along the two crystallographic directions $\rho_{\parallel c}$ and $\rho_{\perp c}$ is shown in Fig. 4. As reported in Ref. 25 Resistivity behavior is typical of this compound, with a maximum of around 300 K due to the change of conductivity from impurity-based to intrinsic and the associated change in the hole mobility and carrier concentration.²⁵ $\rho_{\parallel c}$ and $\rho_{\perp c}$ follow

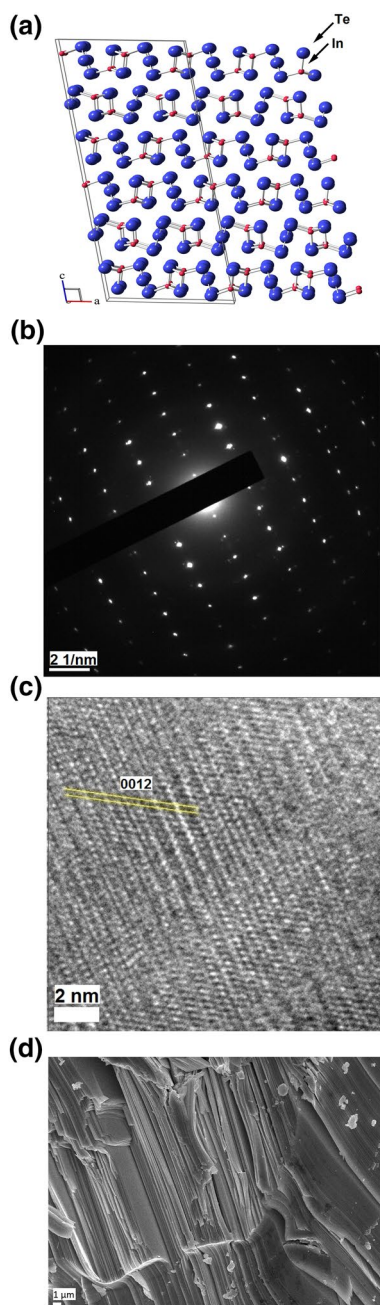


Fig. 3 (a) The crystal structure of In_2Te_5 viewed along the b -axis. (b) The HRTEM selected area electron diffraction pattern, indicating the single-crystalline nature. (c) HRTEM image of the In_2Te_5 single crystal. (d) FESEM image of the layered structure of a monoclinic In_2Te_5 single crystal.

different paths, indicating anisotropic behavior. At about 300 K, $\rho_{\parallel c} = 0.096 \Omega\text{m}$ and $\rho_{\perp c} = 0.12 \Omega\text{m}$. We have measured Hall carrier concentration as a function of temperature for undoped In_2Te_5 , and $\text{In}_2(\text{Te}_{1-x}\text{Se}_x)_5$, $x=0.5, 0.10$, and $\text{Fe}_{0.05}\text{In}_{1.95}(\text{Te}_{0.90}\text{Se}_{0.10})_5$ samples reported by Sanchela et al.³² We have observed extrinsic and intrinsic behavior in mid- and high-temperature regions. The carrier concentration

Table 1 A summary of the crystallographic data and Rietveld refinement parameters for the single crystal of In_2Te_5

Sample	In_2Te_5
Nature	Single crystal
Data	Powder XRD
Crystal Structure	Monoclinic
Space group	C12/c1 (15)
a (Å)	16.375 (5)
b (Å)	4.330 (1)
c (Å)	40.730 (1)
V (Å ³)	2888
R_{exp} %	3.418
R_{pro} %	6.940
R_{wp} %	9.225
χ^2	7.284

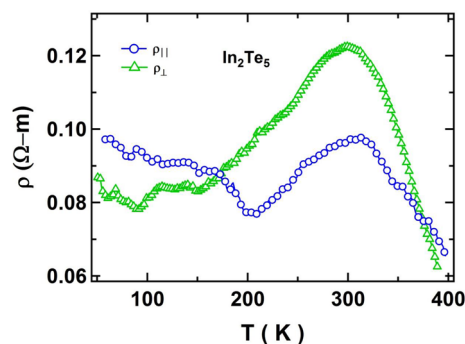


Fig. 4 Variation of electrical resistivity (ρ) as a function of temperature (T) for In_2Te_5 single crystal, parallel and perpendicular to the c -axis.

increased as the doping content was increased. We show that undoped In_2Te_5 has a very low carrier concentration. The maximum carrier concentration was in the range of $\sim 10^{10} \text{cm}^{-3}$. As a result, poor electrical transport properties were observed for undoped In_2Te_5 .

Seebeck Coefficient

The variation of the Seebeck coefficient $S(T)$ with respect to temperature along with the two directions, $S_{\parallel c}$, and $S_{\perp c}$, for the single crystal of In_2Te_5 is shown in Fig. 5a. The positive sign of the Seebeck coefficient indicates that the majority of charge carriers are p-type (holes) throughout the temperature range. The highest value of $S_{\parallel c}$ is $480 \mu\text{V/K}$ at about 273 K and $S_{\perp c}$ is $408 \mu\text{V/K}$ at about 267 K. During the initial increase in temperature, $S(T)$ both the orientations remain the same, but after about 200 K, $S_{\parallel c}$ increases faster as compared to $S_{\perp c}$ ($S_{\parallel c} > S_{\perp c}$). The maximum in $S(T)$ is in agreement with the maximum observed in the conductivity of this

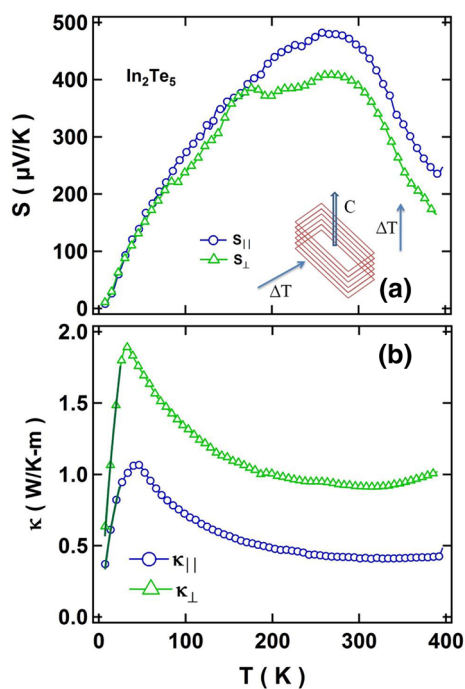


Fig. 5 (a) Variation of Seebeck coefficient (S) and (b) total thermal conductivity (κ) as a function of temperature (T) for In_2Te_5 single crystal parallel and perpendicular to c -axis. The inset in the upper panel shows the schematic diagram of layers and the temperature gradient applied parallel and perpendicular to the c -direction.

sample due to the change of conductivity from impurity-based to intrinsic and the variation of hole mobility and hole concentration with temperature.²⁵

In order to find the energy band gap (E_g) for our crystal, we used the Goldsmid and Sharp formula,²⁷

$$E_g = 2eS_{\max}T_{\max} \quad (1)$$

where e is the hole charge, S_{\max} is the maximum value of the thermopower, and T_{\max} is the corresponding temperature. Using the values of S_{\max} and T_{\max} from Fig. 5a, we calculated $E_g = 0.21$ eV at 267 K and 0.26 eV at 273 K for $S_{\perp c}$, and $S_{\parallel c}$ directions, respectively.

Thermal Conductivity

In order to measure the direction-dependent thermal conductivity, a temperature gradient was applied either along or perpendicular to the c -axis. In the inset of Fig. 5a, the schematic diagram of the layered configuration with a temperature gradient applied parallel or perpendicular to the crystallographic c -axis is shown. The temperature dependence of the total thermal conductivity (κ) along with the two crystallographic directions ($\kappa_{\parallel c}$, and $\kappa_{\perp c}$) is shown in Fig. 5b. Both the thermal conductivities follow the power

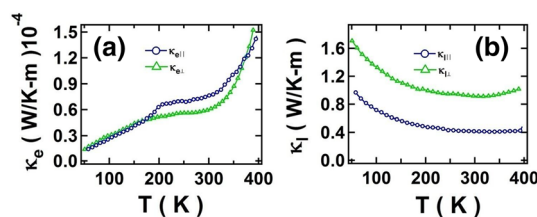


Fig. 6 Variation of (a) κ_e and (b) κ_l with temperature (T) for In_2Te_5 single crystal parallel and perpendicular to the c -axis.

law (the powers being 0.37 and 0.60 for $\kappa_{\parallel c}$, and $\kappa_{\perp c}$, respectively) up to 35 K with a typical phonon Umklapp maximum at ~ 35 K. The total thermal conductivity $\kappa_{\perp c}$ is found to be higher than $\kappa_{\parallel c}$ in the entire temperature range, indicating a clear anisotropy in the conduction process in this compound. At room temperature, these values are $\kappa_{\perp c} = 0.916$ W/m K and $\kappa_{\parallel c} = 0.411$ W/m K. These are comparable to the thermal conductivities of some of the well-studied compounds such as SnSe and²⁰ doped PbTe,²⁸ thus making In_2Te_5 a promising thermoelectric material with a clear anisotropy in the heat-conduction pathway. The anisotropy in thermal conductivity may be attributed to the layered structure²⁴ of the compound with very different lattice parameters. When the thermal gradient is applied perpendicular to the crystallographic c -axis (i.e., along the In-Te planes), the thermal currents encounter an easier path (higher thermal conductivity) as compared to the case when the thermal gradient is applied along the c -axis (i.e., perpendicular to the In-Te planes) due to the gaps between the layers, which are connected only through weak van der Waals interactions.^{12,24,29}

The electronic part of the thermal conductivity (κ_e) is estimated from the Wiedemann-Franz law, $\kappa_e = L_0\sigma T$, where L_0 is the Lorenz number, 2.44×10^{-8} $\text{W}\Omega\text{K}^{-2}$ and σ is the electrical conductivity (obtained from the resistivity curves in Fig. 4). Figure 6a depicts the calculated κ_e values for the two configurations of the applied thermal gradient ($\kappa_{e\parallel c}$ for the parallel direction and $\kappa_{e\perp c}$ for the perpendicular direction) κ_e values in both directions increase with increasing temperature, consistent with the observed resistivity behavior. The lattice thermal conductivity ($\kappa_{l\parallel c}$ for the parallel direction and $\kappa_{l\perp c}$ for the perpendicular direction), after subtracting the electronic part from the total thermal conductivity, is shown in Fig. 6b. It is obvious from the figures that the electronic thermal conductivity is four orders of magnitude smaller than the lattice thermal conductivity, and hence it can be argued that the phonon contributions towards κ is dominant. This is further confirmed by the heat capacity measurements, as shown in Fig. 7, where it is shown that the heat capacity data can be fitted to the standard Debye model in the entire temperature range.³⁰

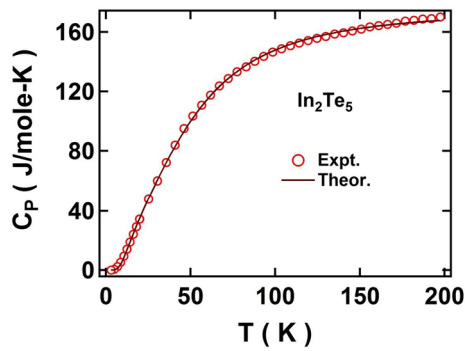


Fig. 7 Measured specific heat (C_p) versus temperature (T) for the In_2Te_5 single crystal. The estimated values from the Debye model are shown as a solid line.

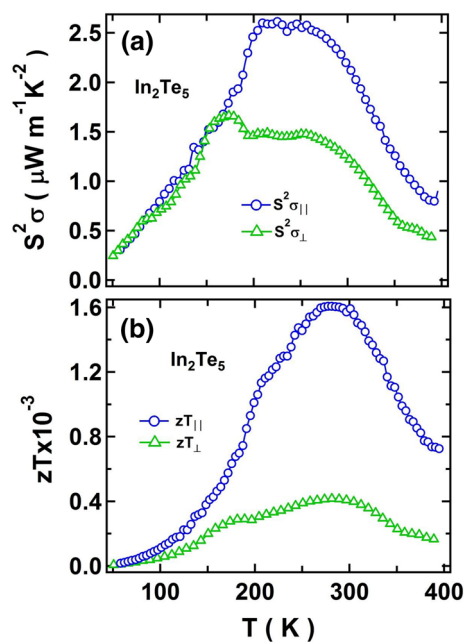


Fig. 8 Variation of (a) power factor ($S^2\sigma$) and (b) figure of merit (zT) as a function of temperature (T) for In_2Te_5 single crystal parallel and perpendicular to the c -axis.

$$C_p = 9R \left(\frac{T}{\theta_D} \right)^3 \int_0^{x_D} dx \frac{x^4 e^x}{(e^x - 1)^2} \quad (2)$$

where R is the gas constant and θ_D is the Debye temperature, $x_D = \left(\frac{\theta_D}{T} \right)$.

The temperature-dependent power factors ($S^2\sigma$) along the two directions ($\parallel c$ and $\perp c$) are shown in Fig. 8a. The power factor increases sharply above ~ 170 K along the $\parallel c$ direction and reaches a maximum value of $2.61 \mu\text{W}/\text{K}^2\text{m}$ at about 225 K as compared to that along the $\perp c$ axis, which has a maximum value of only $1.45 \mu\text{W}/\text{K}^2\text{m}$. The temperature-dependent figure of merit (zT) along with the two directions $zT_{\parallel c}$ and $zT_{\perp c}$ is shown in Fig. 8b. $zT_{\parallel c}$ increases with temperature with a peak value of 1.6×10^{-3} which is ~ 4 times larger than the $zT_{\perp c}$ (4.1×10^{-4}) at about 270 K. The summary of composition and room temperature values of thermal conductivity (κ), resistivity (ρ), Seebeck coefficient (S), band gap (E_g) and figure of merit (zT) for the In_2Te_5 single crystal in different directions are shown in Table II.

Conclusions

We have successfully grown single crystals of In_2Te_5 . By the thermopower measurements, we conclude that the majority of the charge carriers are holes. We have calculated the band gap through the Goldsmid and Sharp formula, which suggests that In_2Te_5 could be considered a narrow-band semiconductor. We have observed using direction-dependent studies that the lattice thermal conductivity along the $\parallel c$ direction is smaller by a factor of 2 as compared to the same along the $\perp c$ axis, indicating the role of anisotropy in this material. Similar anisotropic behavior is seen in the thermopower and electrical resistivity of this compound. These, in turn, lead to an anisotropy in power factor and figure of merit. Our studies reveal that, due to anisotropic behavior, bulk material with a layered structure, a large unit cell, and very low thermal conductivity, the In_2Te_5 single crystal is a promising candidate in providing further scope to develop high-efficiency thermoelectric materials. Even though the overall figure of merit value is small in this compound, suitable dopants can be used to investigate whether the electrical transport properties can be enhanced. Another

Table II A summary of composition and room temperature values of thermal conductivity (κ), resistivity (ρ), Seebeck coefficient (S), band gap (E_g) and figure of merit (zT) for the In_2Te_5 single crystal in different directions

Nominal composition	Average composition by EDAX	Direction	κ (W/Km)	ρ (Ωm)	S ($\mu\text{v}/\text{K}$)	E_g (eV)	zT
In_2Te_5	$\text{In}_{2.08}\text{Te}_{4.92}$	$\parallel c$	0.41	0.096	460	0.27	1.6×10^{-3}
		$\perp c$	0.92	0.12	392	0.23	4.0×10^{-4}

aspect that can be improved to obtain higher values of the figure of merit at higher temperatures is the suppression of the thermopower peak altogether or shifting it to higher temperatures.³² Since In_2Te_5 has a layered zigzag structure that allows electrons and phonons to travel independently, electrons can effectively move inside the layers, but phonons can scatter widely across the layers because of weak van der Waals forces. In short, doping, hot pressing, nanostructuring, alloying, and monolayer approaches are some of the ways that can be combined with layered structure to provide a reduction in thermal conductivity with an optimum zT value.

Acknowledgments CVT would like to acknowledge the Department of Science and Technology for partial support through the project IR/S2/PU-10/2006.

Conflict of interest The authors declare that they have no conflict of interest.

References

- G.S. Nolas, J. Sharp, and H.J. Goldsmid, *Thermoelectrics: Basic Principles and New Materials Developments* (Berlin: Springer, 2001).
- C. Wood, *Rep. Prog. Phys.* 51, 459 (1988).
- T. M. Tritt, M. Kanatzidis, G. Mahan, and H. B. Lyon, *Mater. Res. Soc. Symp. Proc.* 478, (1997).
- K. Koumoto, and T. Mori, *Thermoelectric nanomaterials: materials design and applications* (Berlin: Springer, 2013).
- P. Vaquero, and A.V. Powell, *J. Mater. Chem.* 20, 9577 (2010).
- C. Wan, Y. Wang, N. Wang, W. Norimatsu, M. Kusunoki, and K. Koumoto, *Sci. Technol. Adv. Mater.* 11, 044306 (2010).
- J.L. Cohn, G.S. Nolas, V. Fessatidis, T.H. Metcalf, and G.A. Slack, *Phys. Rev. Lett.* 82, 779 (1999).
- Q. Zhanga, B. Liaob, Y. Lana, K. Lukasc, W. Liua, K. Esfarjanib, C. Opeilc, D. Broidoc, G. Chenb, and Z. Rena, *PNAS* 110, 13261 (2013).
- B. Poudel, Q. Hao, Y. Ma, Y. Lan, A. Minnich, B. Yu, X. Yan, D. Wang, A. Muto, D. Vashaee, X. Chen, J. Liu, M.S. Dresselhaus, G. Chen, and Z. Ren, *Science* 320, 634 (2008).
- L.D. Zhao, S.H. Lo, J. He, H. Li, K. Biswas, J. Androulakis, C.I. Wu, T.P. Hogan, D.Y. Chung, V.P. Dravid, and M.G. Kanatzidis, *J. Am. Chem. Soc.* 133, 20476 (2011).
- C. Nethravathi, C.R. Rajamathi, M. Rajamathi, R. Maki, T. Mori, D. Golberg, and Y. Bando, *J. Mater. Chem. A* 2, 985 (2014).
- J.R. Sootsman, D.Y. Chung, and M.G. Kanatzidis, *Angew. Chem. Int. Ed.* 48, 8616 (2009).
- P. Larson, S.D. Mahanti, D.Y. Chung, and M.G. Kanatzidis, *Phys. Rev. B* 65, 045205 (2002).
- D.L. Medlin, Q.M. Ramasse, C.D. Spataru, and N.Y.C. Yang, *J. Appl. Phys.* 108, 043517 (2010).
- X. Yan, B. Poudel, Y. Ma, W.S. Liu, G. Joshi, H. Wang, Y. Lan, D. Wang, G. Chen, and Z.F. Ren, *Nano Lett.* 10, 3373 (2010).
- R. Venkatasubramanian, E. Siivola, T. Colpitts, and B. O'Quinn, *Nature* 413, 597 (2001).
- S. Lee, J. In, Y. Yoo, Y. Jo, Y.C. Park, H.J. Kim, H.C. Koo, J. Kim, B. Kim, and K.L. Wang, *Nano Lett.* 12, 4194 (2012).
- D. Jung, K. Kurosaki, Y. Ohishi, H. Muta, and S. Yamanaka, *Mater. Trans.* 53, 1216 (2012).
- M.H. Lee, K.R. Kim, J.S. Rhyee, S.D. Park, and G.J. Snyder, *J. Mater. Chem. C* 3, 10494 (2015).
- L.D. Zhao, S.H. Lo, Y. Zhang, H. Sun, G. Tan, C. Uher, C. Wolverton, V.P. Dravid, and G. Kanatzidis, *Nature* 508, 303 (2014).
- M. Taniguchi, R.L. Johnson, J. Ghijsen, and M. Cardona, *Phys. Rev. B* 78, 104204 (1990).
- P. Jood, and M. Ohta, *Materials* 8, 1124 (2015).
- P.D. Walton, H.H. Sutherland, and J.H.C. Hogg, *Acta Cryst. B* 34, 41 (1978).
- X. Shi, J.Y. Cho, J.R. Salvador, J. Yang, and H. Wang, *Appl. Phys. Lett.* 96, 162108 (2010).
- M.M. Nassary, M. Dongal, M.K. Gerges, and M.A. Sebage, *Phys. Stat. Sol. (a)* 199, 464 (2003).
- E.G. Grochowski, P.R. Mason, G.A. Schmitt, and P.H. Smiths, *J. Phys. Chem. Solids* 25, 551 (1964).
- H.J. Goldsmid, and J.W. Sharp, *J. Electron. Mater.* 28, 869 (1999).
- K. Biswas, J. He, I.D. Blum, C.I. Wu, T.P. Hogan, D.N. Seidman, V.P. Dravid, and M.G. Kanatzidis, *Nature* 489, 414 (2012).
- J.S. Rhyee, K.H. Lee, S.M. Lee, E. Cho, S. Kim, E. Lee, Y.S. Kwon, J.H. Shim, and G. Kotliar, *Nature* 459, 965 (2009).
- C. Kittel, *Introduction to Solid State Physics*, 7th ed., (New York: John Wiley, 1996).
- W. Zhang, N. Sato, K. Tobita, K. Kimura, and T. Mori, *Chem. Mater.* 32, 5335 (2020).
- A.V. Sanchela, A.D. Thakur, and C.V. Tomy, *J. Electron. Mater.* 45, 5540 (2016).

Publisher's Note Springer Nature remains neutral with regard to jurisdictional claims in published maps and institutional affiliations.